Received: 26 July 2023 | Revised: 23 October 2023 | Accepted: 22 November 2023
DOI: 10.1111/ffe.14209

ORIGINAL ARTICLE

FFEMS Fatigue & Fracture of Engineering Materials & Structures
WILEY

Martensite content effect on fatigue crack growth and fracture energy in dual-phase steels

D. Avendaño-Rodríguez[1] | **R. Rodriguez-Baracaldo**[2] | **S. Weber**[3] | **L. Mujica-Roncery**[4]

[1]Research Group: Diseño Avanzado, Fundación Universidad de América, Bogotá D.C., Colombia

[2]Research Group: Innovación en Procesos de Manufactura e Ingeniería de Materiales, Universidad Nacional de Colombia, Bogotá D.C., Colombia

[3]Institut für Werkstoffe, Ruhr-Universität Bochum, Lehrstuhl Werkstofftechnik, Bochum, Germany

[4]Research Group: Grupo de Investigación en Materiales Siderúrgicos e INCITEMA, Universidad Pedagógica y Tecnológica de Colombia, Tunja, Boyacá, Colombia

Correspondence
R. Rodriguez-Baracaldo, Universidad Nacional de Colombia, Car. 30 No 45-03, Bogotá D.C., Colombia.
Email: rodriguezba@unal.edu.co

Abstract

The effect of different microstructural factors on crack growth and fatigue fracture mechanisms in dual-phase (DP) steels has yet to be fully understood. The present research examines the relationship between crack growth, microstructure, and fracture mechanisms. The samples were intercritically annealed at different temperatures to produce three different martensite volume fractions (MVFs). The results show that the mechanical incompatibility of ferrite and martensite promotes continuous crack tip deflection. MVF increases are associated with elevated fracture tortuosity, more significant fracture energy surface formation, and higher Paris law exponent m values. The interaction of the microstructure with the crack tip, the strain energy density, and the softening caused by secondary microcrack propagation are all illustrated by Electron backscatter diffraction (EBSD) maps. Increasing MVF promotes slow crack growth and a fracture energy increase of 22.9% between the as-received and heat-treated steels.

KEYWORDS

crack propagation, dual-phase steels, EBSD, fatigue, martensite volume fraction

Highlights

- Martensite content in dual-phase steels generate greater crack propagation resistance.
- Martensite volume increase produces a more significant number and extension of secondary microcracks.
- Differences in ferrite and martensite phases promote continuous crack tip deflection.

1 | INTRODUCTION

The development of new types of advanced high-strength steels (AHSS) has recently been made possible by the industrial requirement for materials that increase the mechanical resistance and safety of newly designed vehicles and structures.[1] Dual-phase (DP) steels are part of the first family of AHSS and are in great demand as construction materials for metallic structures because of their low carbon content, good formability, and low production costs.[2] Intercritical heat treatments followed by quenching are typically applied to create DP steels. The

Abbreviations: MVF, martensite volume fraction; AR, as received; HT, heat treatment.

resulting microstructure consists of a ferrite matrix with dispersed martensite grains. Different studies have shown that increased intercritical heat treatment temperatures have two main effects on the martensite properties: They increase the volume fraction and enhance its ductility.[3,4] Different researchers have also reported that DP steel exhibits the best mechanical properties, between 20% and 40% martensite content.[5,6] In addition, an interesting set of characteristics such as low yield point, high ultimate tensile strength, strain hardening, good fatigue resistance, and good weldability have allowed DP steel implementation to be widely extended in different structural applications.[7,8]

Due to the particular use of DP steels in the automotive industry, some research has focused on investigating the DP fatigue behavior in the presence of flaws and cracks. Previous studies reported that DP fatigue crack growth depends on four aspects: stress intensity factor, mean stress, load ratio, and environmental conditions.[9] In addition, some fatigue crack propagation results revealed a strong influence of microstructure on crack growth rates: a more meandering crack path is favored by coarse ferrite-martensite morphologies, which significantly increases long crack propagation fatigue resistance.[10] Moreover, martensite volume fraction (MVF) and crack growth rate affect the crack shape. The crack path is severe and broad at higher rates, whereas the form is narrow and zigzag at lower rates.[10,11]

Concerning the stress field and the damage accumulation in the microstructure, several researchers mention that the deformation is not uniform due to the martensite distribution, interconnection, and volume fraction, concentrating mainly on the ferrite grains. Furthermore, plastic deformation initially surrounds martensite grains before eventually spreading through them as the deformation process increases.[12] According to Bartz et al.'s research, martensite distorts the fracture trajectory and disrupts the homogeneity of the deformation process. Furthermore, thick grains promote crack growth, while grain crystallographic orientation changes inhibit the spread of cracks.[13] According to Bag et al., a uniform distribution of phases and grain sizes improves ductility and toughness in DP steels. They also assert that the martensitic banding structure generated during rolling processes favors crack propagation in the case of martensite with coarse grain sizes. As a result, as the martensite grain refines and the ferrite is free of precipitates, the material toughness increases.[14] A low MVF favors ferrite cleavage or quasi-cleavage fracture, whereas medium and high martensite content tends to form a more ductile fracture with increasing surface dimples.[14–16]

According to Kumar et al., microscale phenomena involving dislocation slippage and the discrete nature of plastic flow determine crack nucleation, crack growth, and microstructure flow resistance. They also show that changing the crystallographic orientation of each grain in the microstructure can slow down crack propagation because the initial propagation plane does not coincide with the grain orientation in the crack front.[17] Furthermore, the crack front does not propagate similarly in different grains due to two phases in the microstructure. For instance, while in ferrite, the crack advances straight, and the plastic zone expands in size as it crosses the grain due to the emission of dislocations from the crack front, in austenite, the crack propagates in a zigzag due to the activation of multiple slip systems.[17] Shi et al. state that low-angle grain boundaries ($<15^\circ$) provide an easy path for dislocation slip and crack propagation because the slip systems on each side of the boundary are nearly coplanar. High-angle grain boundaries, in contrast, are more disordered and have higher interfacial energy, implying dislocation stacking, strain hardening, and crack direction change, even shifting the transgranular fracture mechanism to intergranular or vice versa.[18]

Under cyclic loading conditions, a crack generated by tensile forces will open, and the crack tip will flow plastically. However, due to the differences between crystal orientations and slip systems, dislocations cannot flow from one grain to the next. As a result, dislocations pile up at grain boundaries, causing stress concentration and strain hardening. Subsequently, due to the external force, dislocations near grain boundaries begin to move, and crack growth becomes transgranular. The elastically deformed material outside the plastic zone at the crack tip recovers during the unloading stage, while the material inside the plastic zone remains deformed, generating compressive stresses. The process continues, and the effective crack length increases, leaving fatigue striations on the fracture surface.[19–21]

Studying the crack growth rate da/dN against the logarithm of the alternating stress intensity factor $\Delta K = K_{max} - K_{min}$ at the crack tip, the curve has a sigmoidal form with three regions. The center region corresponds to the Paris–Erdogan type of power-law relation between da/dN and ΔK (Equation (1)). The lower limit on the cyclic stress intensity factor in the region denotes a threshold value below which the crack does not propagate, called the stress intensity factor range threshold ΔK_{th}, representing an inherently safe design against fatigue. However, ΔK_{th} is much less than their fracture toughness for many metals, so employing these metals at such low ΔK values restricts their utilization.[21,22] Finally, based on the previous stage, fractures occur via rapid unstable crack propagation due to reduced material supporting the force. In the region of stable crack growth, the fracture surface of DP steels is characterized by fatigue striations and secondary cracks; in the region of rapid growth, the fracture mechanisms are cleavage coupled with a ductile fracture.[23]

$$\frac{da}{dN} = C\Delta K^m \tag{1}$$

where da/dN represents the crack growth rate, ΔK is the stress intensity factor range, and C and m are empirical constants that depend on the material, environment, and test conditions, such as the load ratio R, the waveform, and test temperature. Some reported results on DP steels have shown that the magnitude of the exponent m rises with the MVF, whereas the proportionality constant C behaves inversely.[14,16] Other studies show different magnitudes in the constants m and C,[23] or opposite behaviors concerning the martensite content, even with similar carbon content.[24]

According to some studies, as the MVF increases, ΔK_{th} rises, and fatigue crack growth is reduced.[23] In contrast, other studies show that if the ferrite volume fraction is high, the ductility of the steel improves, increasing the fatigue life.[24] Moreover, two fundamental mechanisms are suggested to be the causes of the decrease in the fatigue crack growth in DP steels: a lower carbon content in the martensite generated at high intercritical annealing temperatures and roughness-induced crack closure. Due to the higher toughness of low-carbon martensite, crack front rounding and deflection mechanisms work well to reduce the propagation driving force. In addition, fracture surface asperities, produced by shear strains, inelastic crack tip deformation, and surface oxidation processes, lead to the roughness-induced crack-closure effect.[25]

As can be seen, fatigue crack growth is a very complex phenomenon, which depends, among other factors, on the volumetric fraction of phases, grain size, phase distribution, grain morphology, martensite carbon content, steel chemical composition, microstructure crystal orientation, and the type of grain boundary. There is yet to be a clear consensus regarding the factors that affect the magnitude and trend of the crack propagation parameters for the Paris law and stress intensity factor range threshold in DP steels. Furthermore, the influence of different microstructural factors on crack growth and the fracture mechanisms related to fatigue loads in this material type still needs to be fully understood. This research establishes a link between crack growth parameters in DP steels, microstructure properties, and fracture mechanisms. Additionally, the present study connects experimental methodologies such as fatigue crack growth, fracture energy measurements, nanoindentation, scanning electron microscopy (SEM), and electron backscattering diffraction.

2 | EXPERIMENTAL PROCEDURE

2.1 | Material and heat treatment

The experimental material is standard hot-rolled DP steel with a 3.4 mm thickness composed of martensite (M) and ferrite (F). The main chemical components in weight percent are 0.066 C, 0.0022 N, 1.219 Mn, 0.135 Cr, 0.988 Si, 0.011 P, 0.007 S, and Fe balance. Optical emission spectroscopy (OES) was used to perform the chemical analysis.

Uniaxial tensile tests, crack growth, and fracture energy tests were performed at room temperature to characterize the material mechanically. The geometries agree with ASTM E8,[26] ASTM E647,[27] and ASTM E1820[28] standards. The outer contour specimens were cut in the rolling direction (RD) using a laser cutting process, and the notches were manufactured by wire electrical discharge machining (EDM) cutting. Each mechanical test specimen group was divided into three samples: as-received material (AR1), heat treatments two (HT2), and three (HT3).

The intercritical region annealing temperatures for obtaining different MVFs from DP steel were established between 703°C and 883°C. This range was determined using thermodynamic calculations performed using the TCFE9 (steels/Fe alloys) Thermo-Calc database (Thermo-Calc Software AB, Solna, Sweden). Next, a Thermolyne 21100 tubular furnace was modified to allow vertical specimen drops into a brine bath with a 0.4 s immersion time. ATP®-641 industrial protective coating application prevented decarburization. Before the heat treatments, all specimens were coated twice. Then, a two-step intercritical treatment was implemented to obtain DP microstructures with different MVFs. First, to obtain a fully martensitic microstructure, the specimens were heated to 975°C at a heating rate of 0.6°C/s for 35 min, followed by brine quenching at room temperature (10% NaCl in aqueous solution). Subsequently, HT2 and HT3 materials were subjected to intercritical temperatures of 813°C and 839°C for 30 min, followed by room temperature brine quenching. More details on the microstructure and heat treatment can be found in previous works.[29]

2.2 | Microstructure and nanoindentation

Standard mechanical grinding with SiC paper and polishing procedures were used to prepare the specimens, finishing with a 1.0 μm diamond suspension. After polishing, the specimens were etched in a 3% Nital solution. Olympus BX60 M optical microscopy (OM) and TESCAN MIRA3 SEM were used to examine the microstructure. Furthermore, a MATLAB® algorithm was implemented to do the microstructure quantitative metallographic analyses on three micrographs of each specimen. The material micrograph from the transverse direction is shown in Figure 1.

The load–penetration depth curves for ferrite and martensite were obtained using a Nanomechanics Inc. iMicro tester with a Berkovich diamond indenter. The specimens were indented using a ten-by-ten grid at a step size of 10 μm, with a load of 20.0 mN, and an indentation depth of 450.0 nm. Afterward, the surfaces were etched with a 3% Nital solution for 10.0 s, and the indentation number and phase identification were performed using optical microscopy to define the hardness of each grain.

2.3 | Mechanical test

A Shimadzu UH-500kNI hydraulically driven machine performed the uniaxial tensile tests at a constant cross-head displacement rate of 1.0 mm/min. Specimens were prepared following the ASTM E8 standard [27], with a gauge length of 25.0 mm, and the strain was measured with an Epsilon 3542 axial extensometer.

In addition, crack propagation was studied in compact tension (CT) specimens using a Baldwin SF-10-U fatigue machine, with a sinusoidal dynamic load superimposed on a static load to maintain a constant load ratio. Figure 2 shows the geometry of the crack propagation and fracture energy specimens. A DINO LITE

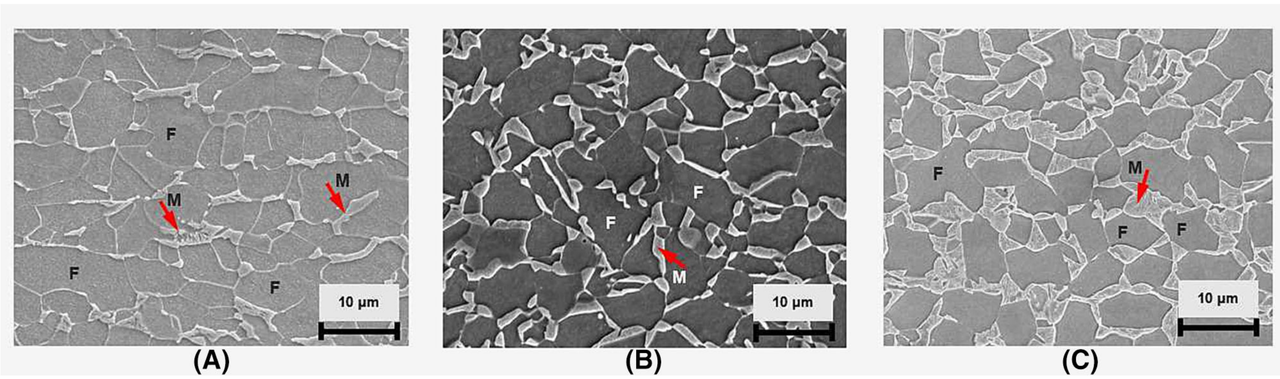

FIGURE 1 Scanning electron microscopy (SEM) micrographs: (A) AR1 17.6% martensite volume fraction (MVF), (B) HT2 31.5% MVF, (C) HT3 47.5% MVF. F denotes ferrite and M martensite. [Colour figure can be viewed at wileyonlinelibrary.com]

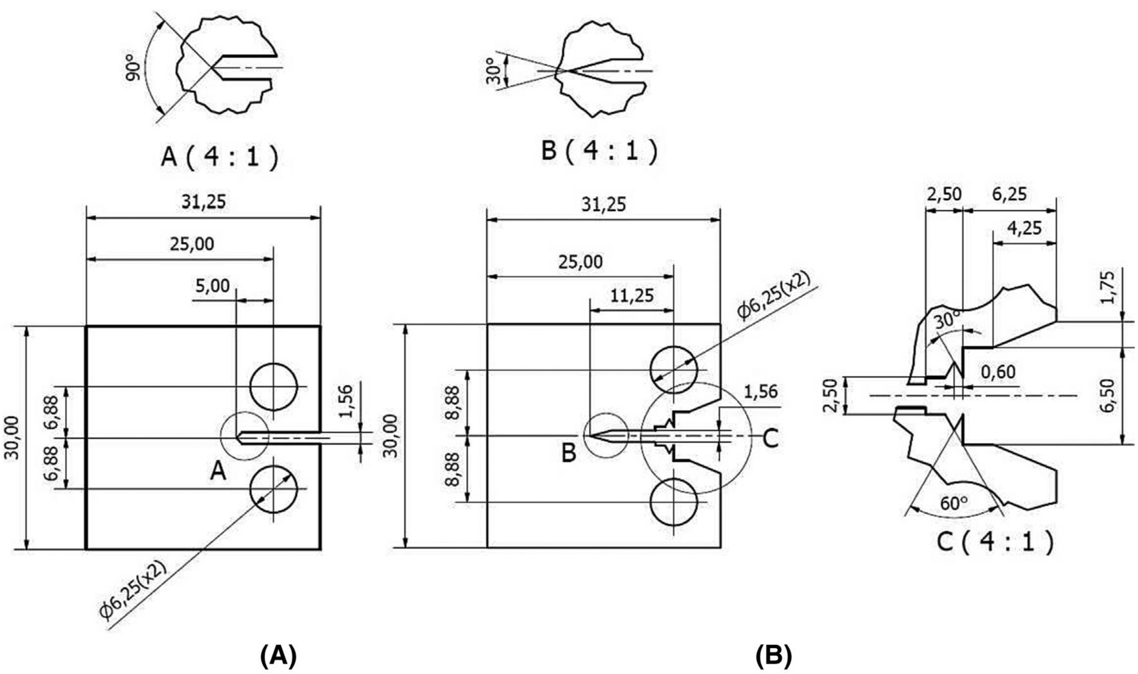

FIGURE 2 Specimen geometries: (A) crack growth compact tension (CT) and (B) fracture energy CT.

AM7115MZT digital microscope installed close to the surface of the specimen was used to measure the crack propagation length. The microscope was set to a magnification of 35X and a distance to the specimen surface of 16.0 mm, resulting in a 9.8 × 7.3 mm observation area and a detailed image of the notch zone and crack tip. In addition, image capture was performed every 10.0 s with Dino Capture 2.0 software, and crack growth measurement was performed on each recorded image using GIMP 2.10.32 software.

Table 1 summarizes the load parameters used in the fatigue experiment. For fatigue experiments, it is critical to ensure that the fracture propagates parallel to the notch and perpendicular to the direction of the load with a minimum angular deviation; otherwise, the test should be invalidated.

In the case of fracture energy measurement, a pre-cracking of 1.25 mm was applied to each of the specimens. Subsequently, they were fractured by employing a uniaxial tensile test at a constant crosshead displacement rate of 0.5 mm/min. The specimen notch crack mouth opening displacement (CMOD) was measured using an Epsilon COD Gage 3541-020M-040M-ST clip-type extensometer with a gauge length of 2.5 mm.

The completely randomized design of the crack propagation and fracture energy tests is carried out for three treatments. The parameters used to carry out the calculation follow a 99% significance level. As a result of the analysis, the number of specimens necessary to achieve power values of 99.98% with an error lower of 1% and a maximum significant difference of 3 times the standard deviation is 10.

2.4 | Electron backscatter diffraction analysis

The crack propagation zone was explored using an electron backscattered diffraction (EBDS) detector coupled to the SEM microscope to observe the interaction of the crack with the microstructure. Additionally, collected data were processed using the AZtec 3.1 analysis software. Excellent image quality was achieved by applying the following EBSD setup parameters: 20 kV accelerating voltage, 1.7 nA beam current, and 85 nm step size. As a result, no image processing was required to clean the resulting EBSD data. To characterize the crack path, different EBDS maps, such as image quality (IQ), inverse pole figure (IP), kernel average misorientation (KAM), and Taylor maps, were used. For the EBSD sample preparation, the procedure consisted of grinding up to 2000 grit SiC sandpaper, followed by polishing up to 0.25 μm with diamond suspension and oxide polishing suspension, finishing in Vibromet for 7 h and final surface cleaning with an ethyl alcohol jet. More details on the EBSD sample preparation can be found in previous work.[29] For the following section, crack tips refer to the singular point at which the crack propagates, and the crack path refers to the route that the crack marks, which can have many changes in direction and can even diverge and generate several routes.

3 | RESULTS AND DISCUSSION

3.1 | Crack propagation and fracture energy in dual phase steels

From the fatigue tests, curves of crack size versus the number of cycles were obtained. Figure 3A shows the crack propagation results of five specimens for each material. AR1 DP steel is colored blue, HT2 green, and HT3 red. Cracks propagate in the material RD. As can be seen, cracks grow faster in as-received material than in heat-treated material within the zone of stable crack propagation. The HT3 material has the most significant crack propagation resistance.

The following procedure was used to find the constants of the Paris equation for each material condition: First, The variation in crack length is evaluated as a function of the number of load cycles applied, resulting in the crack growth rate (da/dN). Second, the variation of stress intensity factor range ΔK as a function of the crack length is evaluated from Equation (2). In this equation, the load range ΔP (see Table 1) and the geometric parameters of the specimen (see Figure 2A) are known; the only unknown term is the crack length produced in each loading cycle.

$$\Delta K = \frac{\Delta P}{B\sqrt{W}} \left[\frac{2+\alpha}{(1-\alpha)^{2/3}}\left(0.886+4.64\alpha-13.32\alpha^2+14.75\alpha^3-5.6\alpha^4\right)\right] \tag{2}$$

where, $\alpha = a$, W is the crack magnitude, W is the distance from the point of load to the opposite side of the notch in the specimen (see Figure 2A), and B is the

TABLE 1 Experimental fatigue test parameters.

Load ratio	Max. load (kN)	Min. load (kN)	Load range (kN)	Static load (kN)	Dynamic load (kN)	Wave
0.1	2.5	0.25	2.25	1.38	1.13	Sinusoidal

thickness of the material (3.4 mm). From Equation (2), it is clear that ΔK depends on the increase of the crack size due to the change of the parameter α in each loading cycle.

Finally, this study employs an adjustment approach with a fourth-degree polynomial to establish a good correlation with the experimental data. Our analysis method was inspired by the previous works of Mohanty et al.[30,31] For each curve, da/dN against ΔK has applied a potential tendency line, obtaining an adjustment equation indicated in Figure 3B for each material. These equations correspond to the Paris law and its parameters, with the coefficient corresponding to the parameter C and the exponent corresponding to the parameter m (see Equation (1)). With the maximum load in Equation (2), a K_{max} of 23.0 MPa.m$^{1/2}$ and with the minimum load a K_{min} of 2.3 MPa.m$^{1/2}$, obtaining a stress intensity factor in the range of 4.8 to 20.7 MPa.m$^{1/2}$.

Different researchers have proposed the following theories to explain the specific relationship between the stress intensity factor range and the crack growth rate: overload,[32] crack closure,[33] microstructural effect[?34], and short crack growth behavior.[35,36] According to Li et al., overload blunted the crack tip, requiring many cycles to reinitiate and propagate the crack. However, this phenomenon involves five stages: the stable period before overload, the instantaneous acceleration period, the delayed retardation period, the retardation period, and the stable period following overload.[32] Figure 3B shows that crack growth increases continuously in the initial process before the slope changes. However, there was no sudden crack size increase before the crack growth slowdown. As a result, the overload effect could be excluded.

Madia et al. explain the phenomenon of slowing fracture growth due to increased crack closure caused by the abrupt production of oxide deposits.[33] At the same time, Wännman et al. indicate that the drop-in growth rate is mainly due to microstructural obstacles. The dip is most likely produced by crack-front deceleration at a hard arrangement of microstructural barriers ?. When considering the effect of martensite on the propagation of cracks in welded joints, Li et al. reach a similar conclusion, as the crack front has to pass through different types of microstructures along its path, forming multiple crack fronts during propagation. Thus, the crack growth rate is arrested.[34]

The final effect to address is that observed by Sadananda et al., who claim that the development of short cracks in the material reduces the rate of crack expansion. The kinetics of crack propagation are controlled by boundaries and changes in the orientation of the crack route, as well as crack arrest until enough damage accumulates to drive the crack past the obstacle for crack lengths proportional to grain size.[35] According to what has been discussed thus far, the mechanical behavior shown in Figure 3B corresponds to a slowing in crack propagation caused by the dual microstructure of ferrite and martensite. Furthermore, the effect is more evident in materials with reduced martensite composition. This last effect can be described by combining crack tip blunting in a ductile matrix with the formation of narrow cracks between ferrite and martensite grains, which reduces the crack growth propagation rate.

Table 2 shows the fitting parameters for the Paris model and the crack propagation test results for each material. The results of the number of cycles to fracture show that the medians of the data are separated,

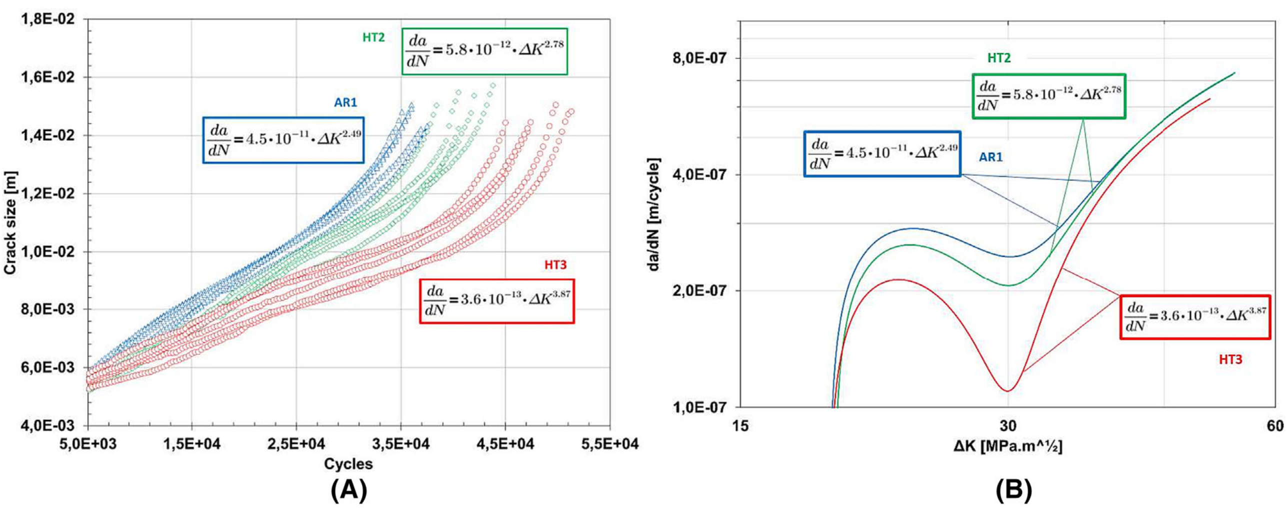

FIGURE 3 Fatigue crack growth curves: (A) crack size versus cycles and (B) crack growth rate versus stress intensity factor range. AR1 17.6% martensite volume fraction (MVF) (blue), HT2 31.5% MVF (green), and HT3 47.5% MVF (red) [Colour figure can be viewed at wileyonlinelibrary.com]

TABLE 2 Fitting parameters for the Paris model.

Material	m	C	Cycles	Total crack length (mm)	ΔK_{th} (MPa.m$^{1/2}$)
AR1	2.49	4.5×10^{-11}	35340.0	14.8	18.4
HT2	2.78	5.8×10^{-12}	44940.0	14.6	18.8
HT3	3.87	3.6×10^{-14}	46066.7	14.4	18.7

Note: m, Paris model exponent; C, Paris model constant; ΔK_{th}, threshold stress intensity factor range.

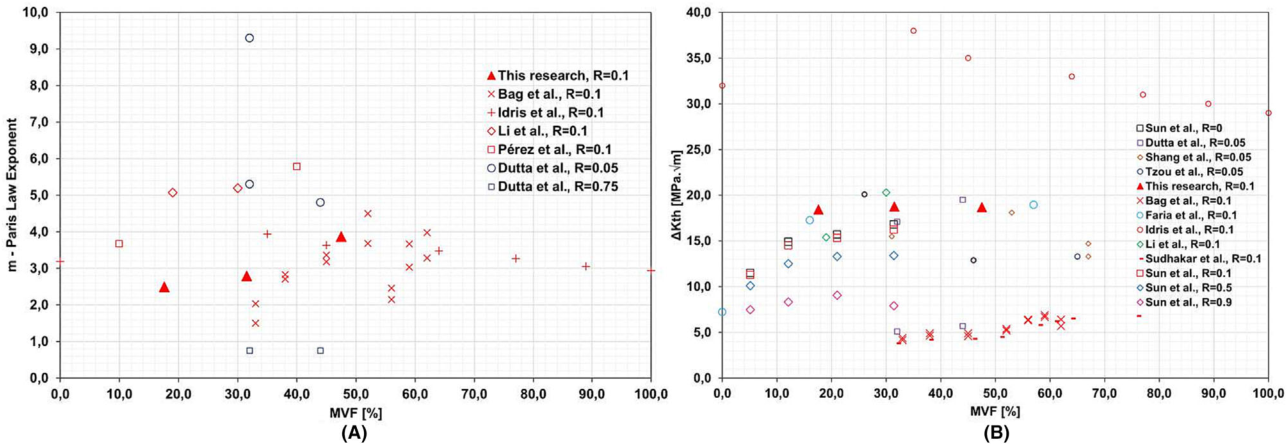

FIGURE 4 Relationship between the fracture parameters and martensite volume fraction (MVF): (A) Paris law exponent. (B) Threshold stress intensity factor range. [Colour figure can be viewed at wileyonlinelibrary.com]

suggesting that intercritical heat treatment affects the number of cycles in the steels. In addition, the medians of the data present an increasing tendency: Thus, the fatigue fracture occurs more slowly with MVF increase, increasing the resistance to crack propagation in the treated materials. If this result is analyzed with those mentioned above, it can be considered that the clear trend in the number of cycles is sufficient proof of the increase in resistance to crack propagation. It is also evident that the experimental measurement method used does not have sufficient sensitivity to conclude the crack length.

Intercritical heat treatment affects the C and m parameters of the Paris law in the steels studied. The medians of C show a decreasing tendency. As the MVF increases, the magnitude of C decreases, slowing fracture development. They were comparing the response of as-received steel with heat-treated steel. Similarly, data statistical analysis allows us to conclude that intercritical heat treatment affects the Paris law parameter m. The medians of the data show an increasing tendency with the MVF increase. Analyzing these two effects in conjunction can gather a global effect of reduction in the crack propagation rate in the treated steels. A significant effect of the heat treatments on the m parameter can be evidenced if the AR1 material is compared against the response of HT2 and HT3. Finally, the optical measurement method used to observe crack growth detects an average crack length of 0.5 mm after 3000 loading cycles. Therefore, ΔK_{th} was determined by identifying the minimum value of the stress-intensity factor range in the Paris curves for each material. All three materials have a similar ΔK_{th} value below which no detectable crack propagation occurs.

Figure 4A shows the behavior of the m parameter of the Paris law versus the martensite content. The data in red were obtained with a stress ratio R of 0.1, while those in blue were obtained with stress ratios of 0.05 and 0.75. Regarding this parameter, the values reported by Idris et al[24] are atypical, showing a decreasing trend in the magnitude of the exponent. Other results seem to be grouped into two sets for the MVF between 8% and 64%. The first set of results gathers the values reported by Bag et al[14,16] and the current investigation with an increasing tendency and magnitudes between 1.2 and 4.6. The second set gathers the results reported by Li et al.,[23] Pérez et al,[37] and Dutta et al,[10] with an increasing trend and magnitudes between 3.6 and 5.8, with an outlier of 9.3. This m parameter, the second most commonly reported in the literature, exhibits an increasing trend with the MVF. However, its magnitude has a wide range. According to the data analysis, there appears to be a relationship between increasing the stress ratio R and decreasing the magnitude of the exponent.

Figure 4B presents the relationship of ΔK_{th} versus the MVF reported by various authors. The data in red color were made with a load ratio R of 0.1, while the other values are indicated next to the author. It is clear that the values obtained by Idris et al[24] are atypical, both for their magnitude and for their decreasing tendency with MVF. Instead, the other data seem to be grouped into three sets for the MVF from 0% to 70%. The first data set, reported by Bag et al[14,16] and Sudhakar et al.[25] (red), shows an increasing trend of ΔK_{th} against martensite content between 30 and 80 $MPa.m^{1/2}$. The second group reported by Dutta et al.,[10] Tzou et al,[38] and Shang et al.[39] (blue) shows a decreasing trend of ΔK_{th}, between 26 and 70 $MPa.m^{1/2}$. The last group shows the results of the present investigation and those of Faria et al.,[40] Li et al,[23] and Sun et al.[41] (red), with a tendency to increase the value of ΔK_{th}, between a range of 5 and 22 $MPa.m^{1/2}$. This last group has in common that the as-received steel has a low carbon content (<0.013% wt. of carbon). It is worth clarifying that in the results of Sun et al,[41] the chemical composition of the steel is not reported, while the material of Faria et al[40] is a chromium steel. Moreover, apart from the chemical composition, the material of the present investigation and that of Li et al[23] has a thickness of less than 3.5 mm. Looking together at all the data in Figure 4B, ΔK_{th} appears to have a parabolic behavior concerning the martensite content, with a maximum of around 35% MVF. Finally, there seems to be a relationship between the increase in the load ratio R and the reduction in ΔK_{th}.

The comparison of the Paris law exponent versus the MVF of the present work (see Figure 4A) is in agreement with the investigation by Bag et al., who indicate that the m parameter increases and C parameter decreases with MVF increase.[14,16] They also indicate that for DP steel with 33% of MVF (similar to HT2), the value of m reported is 2.03, while the value of C is 5.61×10^{-8}. Additionally, for steel with 45% of MVF (similar to HT3), the value of m reported is 3.36, while the value of C is 5.89×10^{-10}. Comparing these reported values with the data in Table 2, it can be seen that the magnitudes of the exponents are similar. However, the constant C differs by several orders of magnitude in the two cases. In the work of Bag et al., cracks propagate faster than steels of this work; however, their steel had 0.16% wt. Carbon and the holding time in the intercritical zone were 60 min. The previous analysis is relevant because the higher carbon content and the longer diffusion time promote the formation of a more significant amount of harder martensite, which could explain the lower resistance to crack propagation reported for the steel in earlier studies.[14,16]

Other researchers agree regarding the incremental behavior of the magnitude of the m parameter. Concerning the MVF increase, Li et al. from steel with 0.08% wt. of carbon obtained two DP steel plates by heat treatment.[23] The first one with 19% of MVF (similar to AR1) presents the following Paris law parameters: $m = 5.074$, $C = 6.22 \times 10^{-12}$, and ΔK_{th}=15.4 $MPa.m^{1/2}$. Also, they produce another steel with 30% of MVF (similar to HT2) with $m = 5.193$, $C = 8.44 \times 10^{-13}$, and ΔK_{th}=24 $MPa.m^{1/2}$. It can be observed that, with the increase of martensite, the parameter m increases while C decreases. Regarding the magnitude of these parameters, it is important to point out that the exponent m parameter reported by Li et al. is approximately double that resumed in Table 2 for AR1 and HT2. In contrast, the C parameter is an order of magnitude minors. Figure 4 shows a wide dispersion in the magnitude of the m parameter concerning MVF reported in the literature.

Finally, ΔK_{th} reported by Li et al. shows an increasing trend with MVF increase, unlike the results presented in Table 2 where it remains constant, although its magnitude is in the range of values indicated by work of Li et al.[23] Some authors report a behavior similar to that reported by Li et al., concerning the parameters C and m,[37] while others report opposite behaviors. For example, Idris et al. in their work, obtained DP steels (25% wt of carbon) through intercritical heat treatments between 748 and 1000 °C, with holding times of 90 minutes,[24] reporting a value of ΔK_{th}=38 $MPa.m^{1/2}$ and m=3.94, for steel with 35% of MVF, while for steel with 45% of MVF, a value of ΔK_{th}=35 $MPa.m^{1/2}$ and m=3.63. It is essential to highlight that both magnitudes, as well as the trend of ΔK_{th} and m reported by Idris et al. are atypical concerning what is commonly reported in the literature since they reduce their magnitude, concerning the MVF increase.[24]

The discussion has shown a spread in range, magnitude, and tendency of crack propagation parameters in DP steels. Different authors report an increase in ΔK_{th} with MVF increase. Sarwar et al. show that ΔK_{th} varies with the MVF. They attribute this phenomenon to the aspect ratio of the ferrite and martensite grains because steels were deformed by a rolling process without a heat treatment to the material to restore the microstructure.[9,11] Sarwar et al. also indicate that when the grain of the two phases is restored, ΔK_{th} is constant.[9,11] The previous discussion explains why, in the present study, an effect of the MVF on ΔK_{th} cannot be appreciated. Instead, Shang et al. report a value of ΔK_{th}=20.1 $MPa.m^{1/2}$ in a steel with 0.08% wt. of carbon and 26% of MVF. They also report a value of ΔK_{th}=18.1 $MPa.m^{1/2}$ in a steel with 0.15% wt. of carbon and 53% of MVF.[39] These ΔK_{th} values suggest again that this parameter presents a moderate variation in magnitude, with the change of MVF and the carbon content in the steel. Other researchers have found a similar behavior to that reported by Shang et al. with appreciable ΔK_{th} variations only in very high values of

MVF[42] or identify the ferrite grain size as responsible for ΔK_{th} variations.[24]

When analyzing reference data, it is straightforward to identify variations in the factors utilized to generate crack propagation tests. The content of carbon and manganese in the steels is in a range of 0.066% to 0.25% and 0.005% to 1.66%, respectively, while the MVF obtained vary from 10% to 100%, with a wide range of heat treatments, which include homogenization of the material when starting from casting raw materials, processes with austenitization and intermediate quenching, austenitization and sequential quenching or austenitization, and intercritical annealing. Of course, heating rates, holding temperatures and times, cooling rates, and quenching media are distributed in a wide range of magnitudes and parameters for these treatments. Additionally, it is also possible to observe that the thicknesses of the most common CT specimens are 6.5 and 12.7 mm. However, this parameter depends to a large extent on the as-received material available to manufacture the specimen, which is why thicknesses of 1.85 and 3.4 mm are also reported. Regarding the load ratio R, it is possible to find a range that includes factors from 0.05 to 0.90, with 0.10 recommended by the ASTM E-647 standard[27]. Although the type of wave applied to the fatigue process that is commonly reported is sinusoidal, the oscillation frequency used varies between 10 and 50 Hz. Low frequencies have been used mainly in thin materials, while for materials with more than 6 mm, frequencies between 20 and 50 Hz have been used.

3.2 | Crack and microstructure interaction

Figure 5 shows the maps corresponding to as received material. Figure 5A shows the IQ map of the intermediate zone. The blue arrow indicates in all these images the direction of lamination of the material. The low number of martensite grains and how the crack has preferential growth through the ferrite grains with very few deflections or bifurcations of cracks can be observed. This propagation arrangement agrees with the results presented in Figure 3 and Table 2. The microstructure offers very little resistance to cracking, which propagates rapidly through the material.

Figure 5C shows in the IPF map a random distribution of crystallographic orientations in the ferrite grains and crack with arbitrary propagation orientation. The martensite can be easily identified on this map since it is poorly indexed (black areas or areas with colored fragments). Figure 5E (KAM map) shows the increase in strain energy in the material by crack propagation. The areas closest to the crack (red) present the highest levels of deformation, while the slip bands are distributed inside the grains (green). Zones near or confined within martensite grains also offer high-strain energy indices. Figure 5G (Taylor map) allows observing areas with less deformation (blue) within the microstructure. It is interesting to highlight that the grains closest to the crack present local orientation variations, which is evidence of the plastic deformation produced and an increase in the density of dislocations within each grain. The ferrite grains next to martensites fractured by the deformation produced during the crack propagation show a residual stress release due to the liberation of energy caused by the microcrack propagation.

Figure 5D shows the final crack propagation and the crack tip with small branching. The interaction of the crack with the microstructure is similar to the one described above, as can be observed in these images. Transgranular propagation with low tortuosity through the ferrite grains is observed. There is a high plastic deformation at the grain boundary with the crack, evidenced by the variation of the crystallographic orientation inside the grains and the strain energy density. Finally, ferrite grains close to fractured martensite grains exhibit stress release due to the propagation of strain cracks.

Three factors can be observed in the trajectory of the crack-producing subgrains: First, the fracture process allows the generation of secondary cracks inside the grain that promote fragmentation and separation. Second, the accumulation of dislocations increasing the strain energy allows the formation of subgrains with different crystallographic orientations within the fractured grains. Finally, the fracture of martensite grains with incomplete indexing allows observing these zones with apparent internal substructures in some material segments.

Figure 6A corresponds to the intermediate zone of fracture of the HT2 material. This figure shows how the crack, now with a more tortuous morphology, offers a more significant interaction with the martensite grains with the MVF increase. Larger areas are affected by plastic deformation due to MVF increase. In Figure 6C, a ferrite grain (red) with orientation [001] can be seen on the upper right. This exact grain in Figure 6E allows observing the effect of energy released by microcracks propagation. Close to areas with the propagation of microcracks, the grain reduces its resistance to plastic flow (blue areas, Figure 6G), and a high strain energy density can be observed inside it (green areas, Figure 6E). Figure 6B, shows how the crack front intercepts several martensite grains and is deflected when approaching a martensite grain backed by a ferrite grain. The crack tip fractures the martensite and is deflected due to a

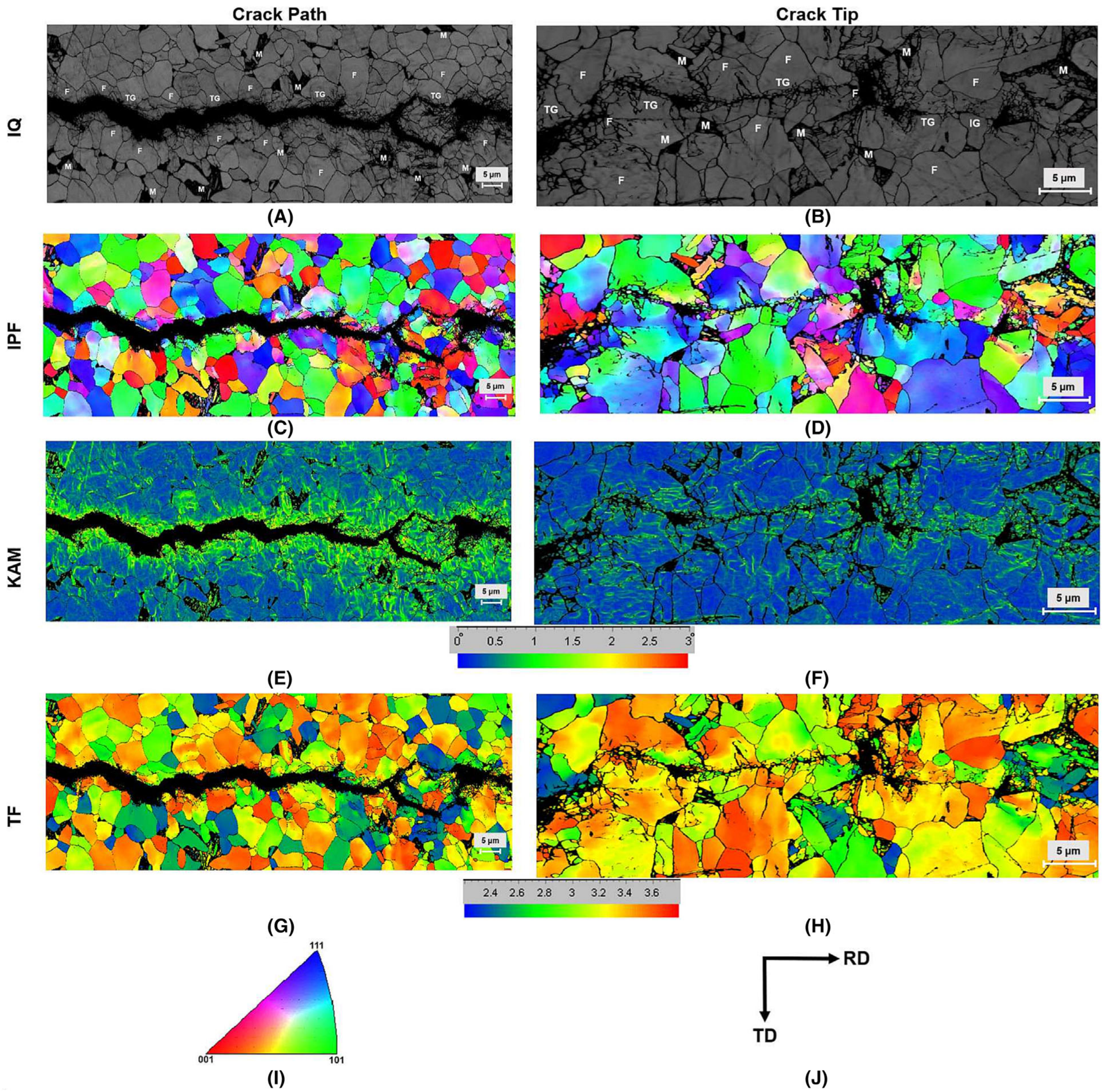

FIGURE 5 EBSD maps of the crack path (A, C, E, G) and crack tip (B, D, F, H) in the as-received material (AR1) after propagation tests, depicting image quality contrast (IQ), inverse pole figure (IPF), Kernel average misorientation (KAM), and Taylor factor (TF) maps. The key for the IPF map (I). Crack growth propagation direction (J). In the image quality maps, F denotes ferrite, M martensite, IG intergranular, and TG transgranular. [Colour figure can be viewed at wileyonlinelibrary.com]

damping effect of the ferrite grain (red arrows Figure 6B). Microcracks propagate within the ferrite grain, dissipating the fracture energy and forcing the crack to follow the route of least resistance. Figure 6F shows an increase in strain energy at the points where the crack is deflected or bifurcated. The differences in toughness and strain between the martensite and ferrite phases become a shield against the crack growth through the microstructure. Also, the crack propagates easily through ferrite in a transgranular manner when the difference in grain size favors this phase. Figure 6H shows again the stress release of the ferrite grains caused by microcracks propagation.

Figure 7A corresponds to the maps of the intermediate zone of the fracture in HT3 steel, showing the increase in martensite grains closest to the crack. Figure 7C shows the crack propagation in a tortuous way through many martensite grains, even generating deformation effects and crystallographic orientation changes in ferrite grains far from the fracture surface. Figure 7E shows the difference in the concentration of strain energy within the material. The zone above the crack has little martensite

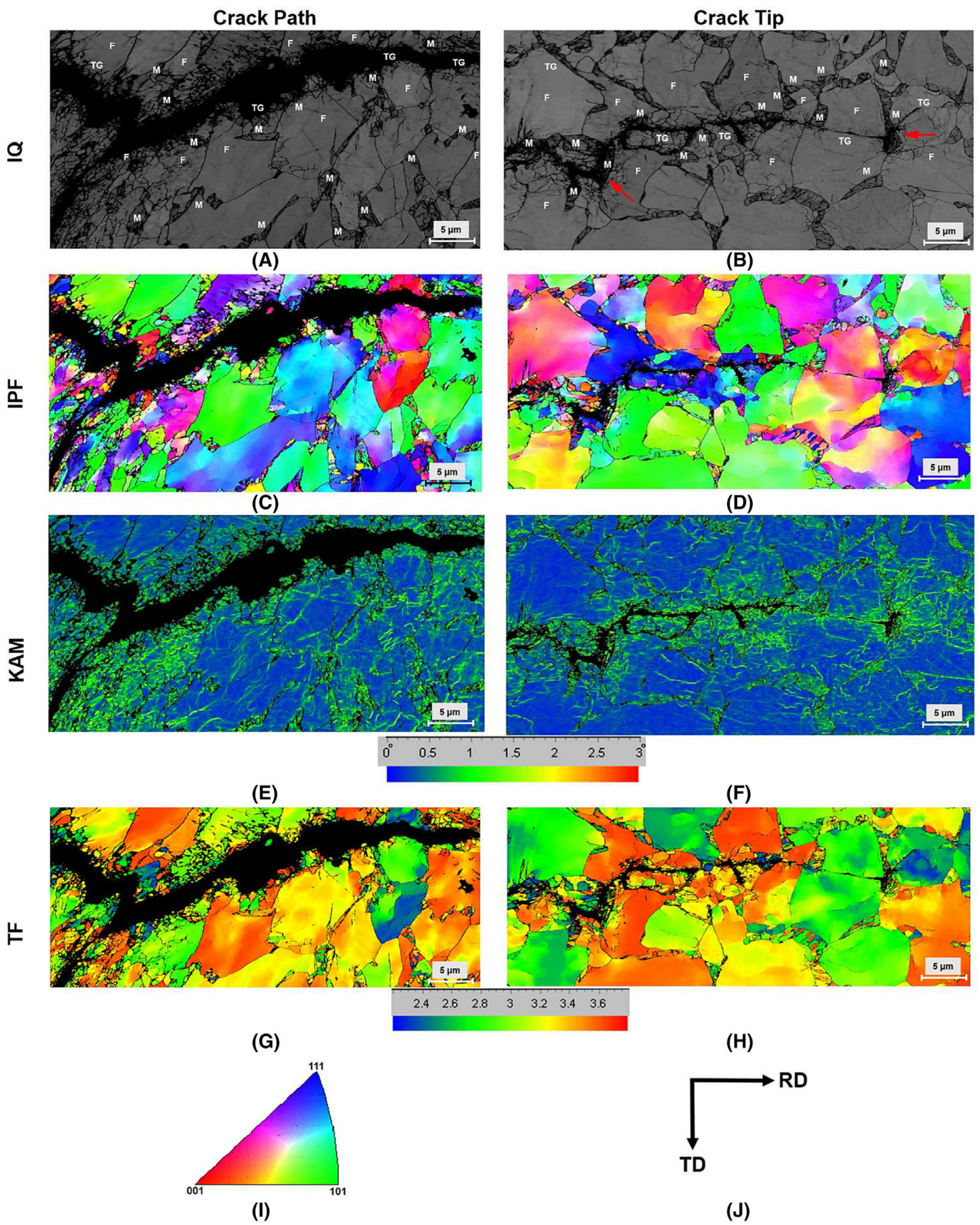

FIGURE 6 EBSD maps of the crack path (A, C, E, G) and crack tip (B, D, F, H) in the intercritical heat treated material (HT2) after propagation tests, depicting image quality contrast (IQ), inverse pole figure (IPF), Kernel average misorientation (KAM), and Taylor factor (TF) maps. The key for the IPF map (I). Crack growth propagation direction (J). In the image quality maps, F denotes ferrite, M martensite, IG intergranular, and TG transgranular. [Colour figure can be viewed at wileyonlinelibrary.com]

grains (and larger ferrite grains). In contrast, the lower area with a higher martensite content has a high density of dislocations caused by the displacement of the crack front and the generation of microcracks. Figure 7G shows that the damage caused by microcracks has spread in large areas with higher martensite content, generating localized stress release in many ferrite grains. Figure 7B corresponds to the crack front of the HT3 steel, showing the tortuosity of the crack through the material. The points where the crack was deflected are indicated with red arrows, zones with martensite grains surrounding the ferrite grain boundaries. As previously shown, the incompatibility of the mechanical properties of the two phases favors the deflection phenomenon, increasing the tortuosity of the crack and the amount of energy needed to propagate it. Figure 7D shows that the crack propagation

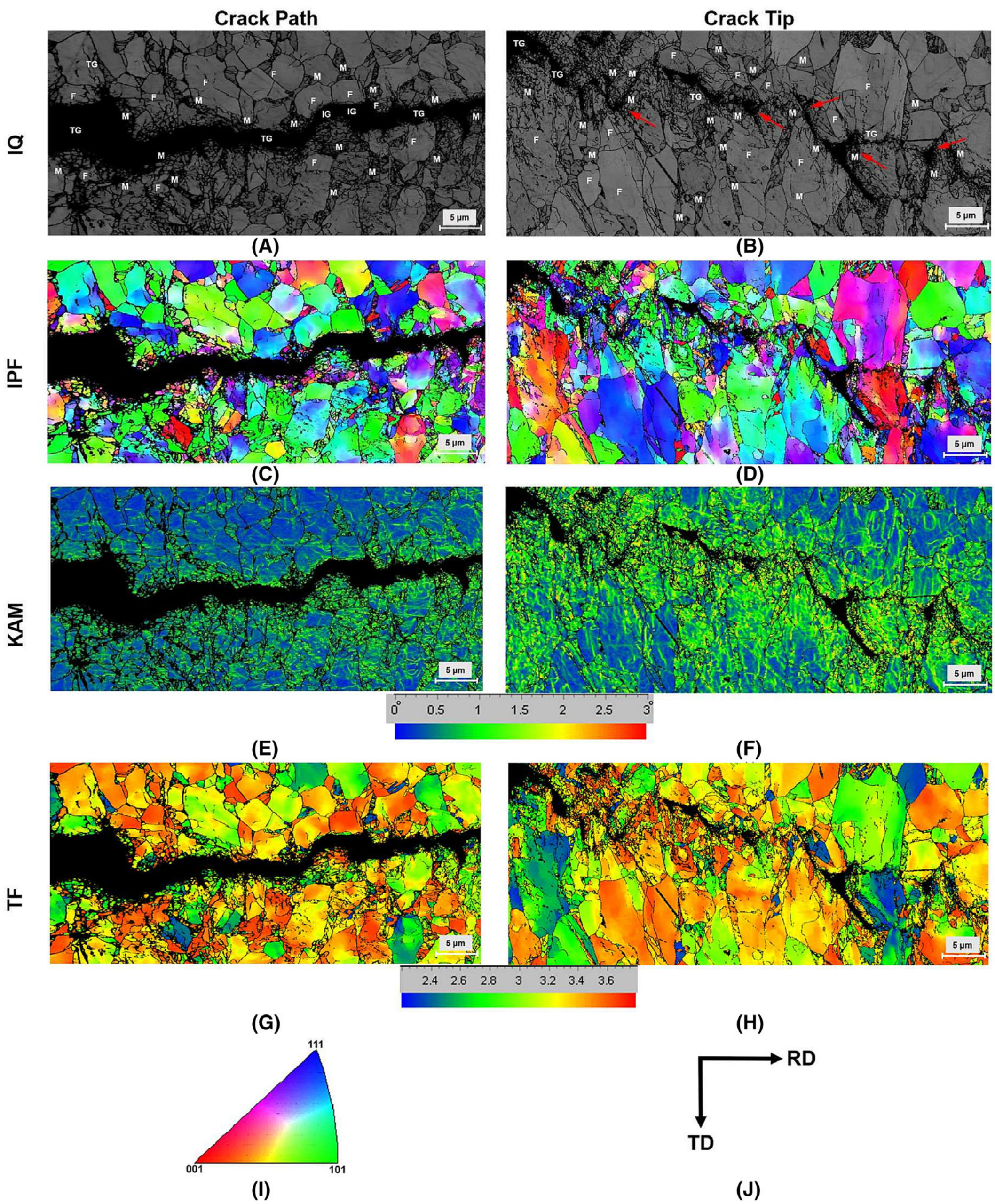

FIGURE 7 EBSD maps of the crack path (A, C, E, G) and crack tip (B, D, F, H) in the intercritical heat treated material (HT3) after propagation tests, depicting image quality contrast (IQ), inverse pole figure (IPF), Kernel average misorientation (KAM), and Taylor factor (TF) maps. The key for the IPF map (I). Crack growth propagation direction (J). In the image quality maps, F denotes ferrite, M martensite, IG intergranular, and TG transgranular. [Colour figure can be viewed at wileyonlinelibrary.com]

affects the crystallographic orientation of most ferrite grains. The formation of these crystalline substructures evidences the high density of dislocations in the crack front and the propagation of cracks within each grain.[43]

It was comparing Figures 5–7; the crack propagates with less velocity in the material with higher martensite content. The MVF increase makes the crack propagation more tortuous and implies more significant plastic deformation and energy necessary to generate the fracture surfaces. The previous analysis also confirmed in Figure 5E since the microstructure has extended stress relaxation due to the energy released by the main crack and the microcracks generated inside the ferrite grains.

Figure 3 is consistent with the interaction of the microstructure with the crack. A higher martensite content generates more significant tortuosity in the crack propagation through the microstructure and implies higher energy needed to create fracture surfaces. Consequently, there is strong evidence that crack propagation is lower in materials with higher martensite content.

The current investigation indicates that the crack propagation rate is lower with increasing martensite content. In this sense, Tayanç et al. reported that as MVF and carbon content increase, fatigue resistance rises, and the crack growth rate of phase dual steels decreases.[44] Tayanç et al. argue that this behavior is caused by a lower carbon content in the martensite generated during the intercritical treatments and the crack closure induced by the roughness of the fracture surface previously generated. The steels they used contained 0.085%, 0.36%, and 0.38% wt of carbon, while the holding time was only 30 min. A significant contribution is that the MVF increase promotes the formation of microcracks at the ferrite-martensite grain boundaries, produced by slip bands adjacent to the interface, reducing energy and speed from the crack front. Moreover, Dutta et al., employing low-stress ratios R, show high values of ΔK_{th} (19 MPa.m$^{1/2}$ and yield stress of 600MPa) associated with the effect of crack closure induced by roughness and the reduction in propagation driving force due to rounding and deflection of the crack front, generating more tortuous crack paths during the propagation process.[10,39]

Sudhakar et al. measured the roughness of the fractured surfaces of steels with MVF between 32% and 76% and established that ΔK_{th} rise with the MVF increase and argue that this phenomenon is relevant on the reduction of crack growth rate in dual phase steels due to the higher fracture energy required. The crack closure resulted from the roughness generated on the fracture surface due to asperities formed by shear stresses, inelastic deformation of the crack tip, and surface oxidation.[25] Additionally, Sudhakar et al. highlight that two factors have a crucial effect on increasing crack closure during propagation. Firstly, the crack will tend to be propagated preferentially in martensite when the content of this phase is high. Since the stress intensity factor range threshold is smaller at the crack front, this makes the crack path more torturous. Secondly, when the crack propagates through a ferrite grain, the surrounding martensite inhibits the ferrite plastic deformation, affecting its crack growth rate as it approaches the martensite grain boundary. Consequently, a large CMOD is required when the MVF increases. The study of Sudhakar et al. seems to confirm the findings of the present research, explaining the differences in fracture behavior in the three types of DP steels tested.[25]

3.3 | Fracture energy in dual phase steels

Figure 8 shows an example of the typical load versus displacement curves for the three types of materials. Because the extensometer only permitted measuring a maximum opening in front of the crack of 2.5 mm, all the curves intersect at this value. It was noticeable that the load required to propagate the damage rises as the MVF increases. The total fracture energy is estimated using Equation (3)[22]:

$$J = \frac{K^2(1-\vartheta^2)}{E} + \frac{2A}{B(W-a)} \tag{3}$$

where K is the stress intensity factor, ϑ is Poisson modulus, E is the elasticity modulus, A is the area under the load versus displacement curve (Figure 8), B is the thickness of the specimen, and $(W-a)$ is the specimen

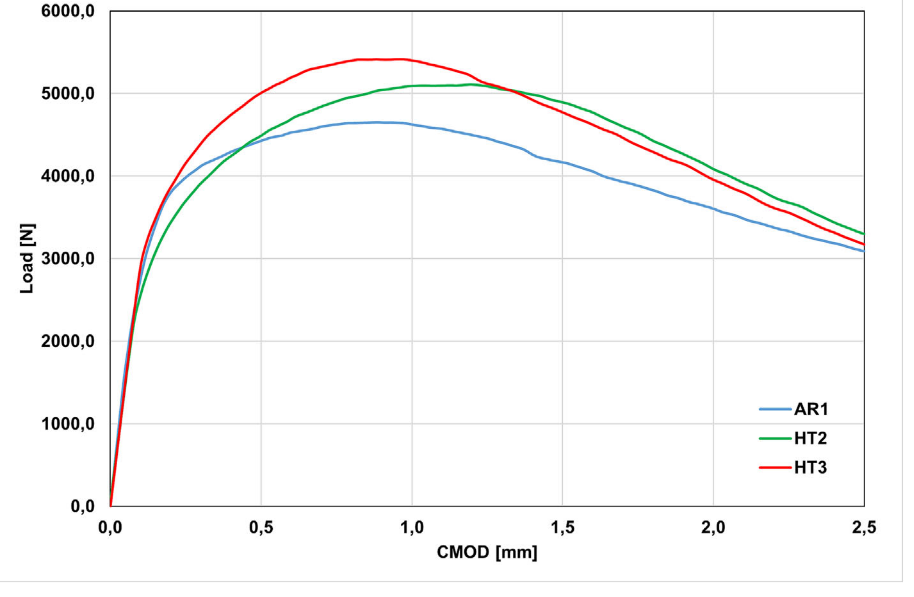

FIGURE 8 Load versus crack mouth opening displacement (CMOD) curves: AR1 17.6% MVF (blue), HT2 31.5% MVF (green), (f) HT3 47.5% MVF (red) [Colour figure can be viewed at wileyonlinelibrary.com]

ligament (See Figure 2B). The elastic energy component of Equation (3) was considered as the load value of the intercept of the curve with a secant line of slope 5%, the modulus of elasticity 210GPa, and 0.3 Poisson modulus. The energy plastic deformation component is computed with the area under the load versus displacement curve of the test for each specimen and some geometric parameters of the specimen. The sum of the elastic and plastic energies (Equation (3)) is the total energy required to propagate a crack in a specimen with a notch of 11.25 mm and a precrack of 1.25 mm. The previous implies that each test was carried out for an effective crack length of 12.5 mm.

Table 3 shows the average of the data obtained from each of the 10 test pieces of each material condition, estimating the fracture energy for each material. The statistical analysis of the results indicates that the data medians are separated and have similar dispersions, implying that the intercritical heat treatment affects the fracture energy of the steels. Furthermore, the medians of the data show that energy rises with the MVF increase. A significant effect of heat treatments on the value of the J integral can be evidenced when comparing the three materials. The energy required to generate the fracture surfaces differs in the three materials (Table 3). The value of the integral J increases as MVF increases. This conclusion verifies prior findings concerning crack propagation velocity and Kernel maps. The rise in MVF causes more tortuosity in crack propagation, requiring more energy to fracture the materials.

Characterizing the fracture energy in DP steels is a research area that requires further development. Very few sources report information related to the fracture energy of DP steels. However, the increase in fracture toughness with the MVF increase has already been reported by some authors.[45,46] This effect is attributed to the fact that by increasing the intercritical heat treatment temperature in steel with a chemical composition fixed, the martensite, although more brittle and harder than ferrite, increases its toughness as a result of reducing its carbon content.[3,46] Although K_{IC} is a parameter used in the literature to indicate the fracture toughness under linear elastic conditions[22,28,47], it is expected to find in the literature the fracture toughness for elastoplastic materials in terms of K_{IC} (See Table 3).

Concerning the magnitude of the fracture toughness in dual phase steels, Tkach et al[46] reported results between 124 and 146 MPa.m$^{1/2}$ with MVF between 20% and 100%. The authors show an increasing linear relationship between fracture toughness and martensite content. Cracks propagated in single-edge notched bend (SENB) specimens at 8 Hz and 0.05 load ratio. The material used in that investigation was DP steel with a chemical composition of 0.06% C, 1.8% Cr, 1.6%Ni, 0.6%Mo (wt).[46] Furthermore, Mosselman work used two steel plates with the chemical composition: 0.092% C, 1.7% Mn, 0.24% Si, 0.032% Al, 0.016% P, and 0.29% C, 1.7% Mn, 0.24% Si, 0.032% Al, 0.016 %P, obtains values for K_{IC} between 71 and 102 MPa.m$^{1/2}$, with MVF between 12% and 95%. In that research, carried out in center crack tension (CCT) specimens at 1 Hz with load ratios between 0.1 and 0.7, an incremental trend between the martensite content and the fracture toughness is again observed.[45] The magnitudes of the K_{IC} value in these two studies demonstrate the same incremental relationship between fracture toughness and martensite content as found in this study. However, the values reported by Mosselman are lower than those reported by Tkach et al. up to 46% for equivalent MVF. Those two studies show differences in composition, specimen type, crack propagation frequency, and load ratio.

Faria et al., with a dual phase steel with chrome and chemical composition: 0.013% C, 0.581% Mn, 0.449% Si, 11.1% Cr, and 0.43% Ni (% wt), show an increasing tendency in the J integral between 0% and 16% of MVF and a decreasing tendency higher than 16% MVF. The reported values are 804 kJ/m^2 (274.8 MPa.m$^{1/2}$) for as-received state without martensite, 1169 kJ/m^2 (324.2 MPa.m$^{1/2}$) for steel with 16% MVF, 713 kJ/m^2 (254.3 MPa.m$^{1/2}$) for 57% MVF, and 94 kJ/m^2 (90.4 MPa.m$^{1/2}$) for 100% martensite.[40] The data in parentheses were estimated for comparative purposes.

Compared with the results of this investigation, it pointed out the MVF as a reference parameter. Faria et al. results for integral J have a magnitude seven times greater in the range from 16% to 18% MVF and 3.5 times higher in the 46% to 57% MVF range. The fatigue test of that research was carried out with identical parameters of this study: load ratio 0.1, crack propagation in the direction of rolling, and type CT specimen (similar in proportions).

TABLE 3 Fracture energy of the dual phase steels.

Material	J_{total} (MPa.m)	CTOD (δ) (mm)	K_I (MPa.m$^{1/2}$)
AR1	2.49	0.141	125.0
HT2	2.78	0.192	125.8
HT3	3.87	0.191	135.2

However, as in this investigation, their specimen does not meet the plane strain condition due to the thickness of the as-received material (6 mm).[40] One reason that may explain the difference in the J integral is the effect of the alloying elements on the mechanical properties, particularly the chromium and nickel elements. Additionally, a reduction in the fracture toughness of DP steels at very high MVF is something that can be expected since, due to the mechanical properties of the martensite phase; cracks will propagate more quickly through the microstructure because the shielding and deflection effects generated by the two phases no longer exist.

The fracture toughness of DP steels is an uncommonly reported property in the literature. Figure 9 shows the results of the references with fracture toughness values. To compare the results, all reported values were converted to K_{IC} using the information reported by the authors on the specimen geometry and mechanical properties. Also, significant variability of the stress intensity factor can be observed, as in the case of the Paris law tests.

Figure 9 shows that the results have two different trends. First, the results of this investigation, Tkach et al.,[46] Mosselman et al[45] and Michizuki et al,[48] present an incremental behavior of the fracture toughness with the MVF increase. It is also interesting to highlight that the equivalent carbon content is close to one of the four material types in this research. Furthermore, the data reported by Faria et al[40] show a decreasing trend in fracture toughness with an MVF increase. The materials of Faria et al. and Qi et al[49] have equivalent carbon contents higher than the rest of the materials. They are chromium and manganese alloying elements, respectively. Therefore, there seems to be a relationship between the hardness provided by the alloying elements and the fracture toughness behavior. Finally, the data reported by Ambrisko et al[50] are atypical for the carbon equivalent and fracture toughness values reported.

The above results show that increasing the MVF promotes crack propagation more slowly in the steel due to the increased fracture tortuosity. It also implies that the energy required to generate fracture surfaces is higher in steel with a higher MVF. Because of the difference in mechanical characteristics between the phases, the DP microstructure enhances the tortuosity of the cracks propagating through the microstructure. Martensite with a lower fracture toughness is responsible for crack propagation.[51] Due to this, the MVF increase promotes crack propagation through this phase, moving from a mechanism of transgranular fracture (typical of ferrite grains in a material with a low MVF) to a mechanism of mixed intergranular and transgranular fracture in martensite grains. When interacting with the crack front, these grains break close to the ferrite grain boundary or into several fragments.

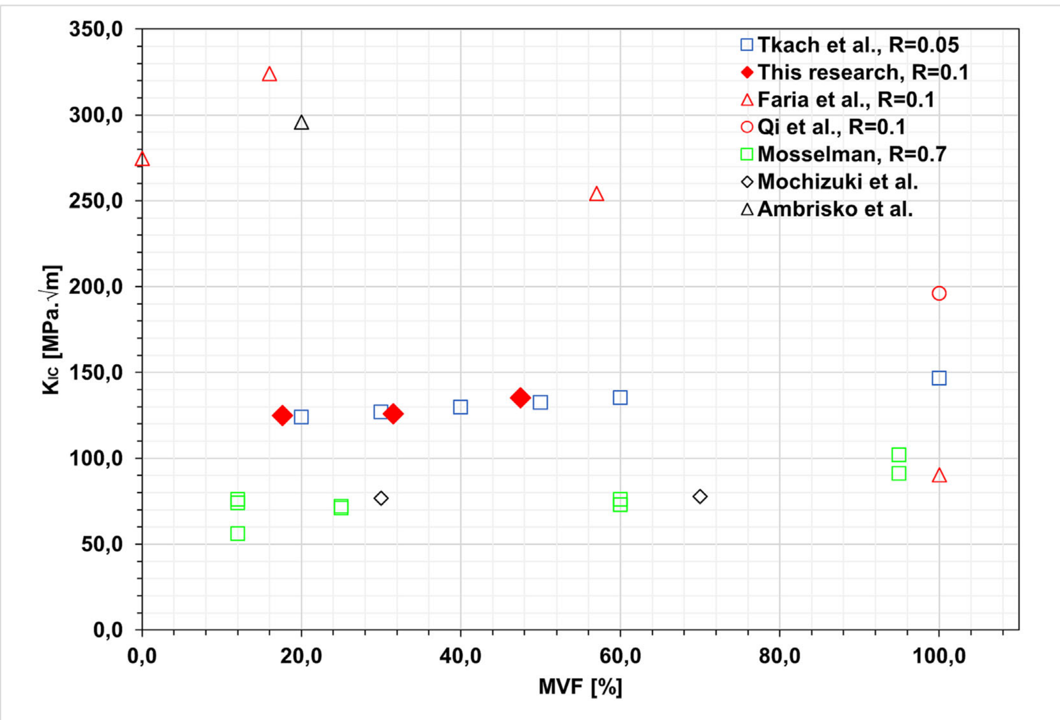

FIGURE 9 Relationship between the fracture toughness and martensite volume fraction (MVF) [Colour figure can be viewed at wileyonlinelibrary.com]

3.4 | Fracture surfaces

Figure 10 shows the fracture surface and striations in the three materials. The blue arrow indicates the propagation direction (common for all images). Figure 10A shows the fatigue deformation process in the AR1 material. Considering material ductility, the striations are fine and hardly visible, presenting different propagation directions depending on the grain they propagate. The behavior is similar for the HT2 material (see Figure 10B). However, the size and number of secondary microcracks are increasing. Moreover, the HT3 material (see Figure 10C) shows the most abrupt topography, with more significant striations and secondary microcracks.[52]

Concerning fatigue fracture surfaces in DP steels with low MVF, Li et al., with the steel of 0.08 %C and 1.66 % Mn (% wt), and MVF between 19% and 30%, indicate that the stable fracture surface is characterized by striations perpendicular to the direction of propagation and frequent secondary cracks in the ferrite grains and in the ferrite-martensite interfaces, that increase in number and length with the increase in the martensite content,[23] similar to the observations in Figure 10. Therefore, they remark that these secondary cracks are responsible for the deceleration of crack growth because they consume the energy of the crack front, and this phenomenon rises when MVF increases.[23]

Figure 10C shows finer initial striations in the lower part, indicating that the spacing of the striations increases with the distance to the point of initiation of the crack; this is due to the reduction of the resistant area of the specimen with the increase of the crack length. In additional work, Li et al. also evidenced this behavior, remarking that the steps in the fracture topography occur when grain boundaries and martensite grains block the propagation process. According to Li et al., due to the difference in crystallographic orientation and the angles of the slip planes when the crack front reaches this point, the crack deviates and loses energy.[34]

Other researchers have studied the fatigue behavior of DP steels with high volumes of martensite fraction. Sudhakar et al., with the steel of 0.14%C, 1.36%Mn and 0.115%Mo (% wt), and a martensite content between 32% and 76%, indicate that at the beginning of the crack growth, the propagation is characterized by transgranular cleavage resulting from the convergence of several propagation fronts, accompanied by secondary cracks that increase with martensite content and are responsible for increasing surface roughness and delaying crack propagation.[25] The fracture morphology described by Sudhakar et al. is the result of the combination of two factors: the chemical composition and the high martensite content obtained. Additionally, Idris et al., with steel of 0.25 %C, 0.634 %Mn and 0.198 % Si (% wt), and MVF between 35% and 100%, report that striations are one of the most notable fracture surface characteristics, with the onset of damage at the ferrite-martensite interface being vital when MVF increases. Idris et al. also remark that the coalescence of microvoids simultaneously combined with striations on the surface is the mechanism of

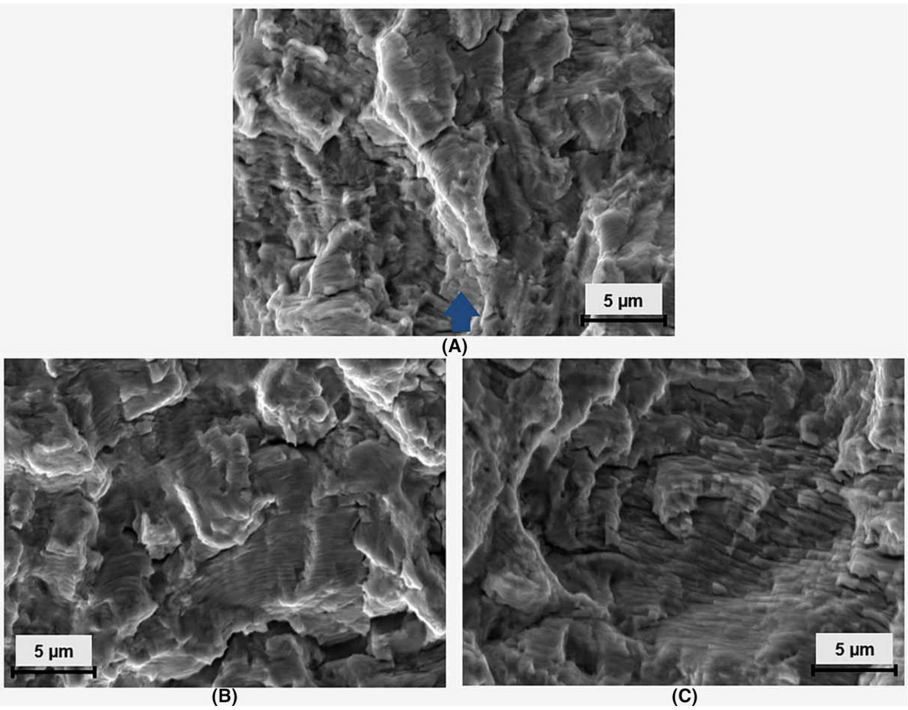

FIGURE 10 Scanning electron microscopy (SEM) micrographs, comparison of fatigue striations: (A) AR1 17.6% MVF, (B) HT2 31.5% MVF, (C) HT3 47.5% MVF. [Colour figure can be viewed at wileyonlinelibrary.com]

transgranular ductile fracture,[24] which can be observed for the HT3 material in Figure 10C. With very high martensite contents, Idris et al. point out that the observed mechanism is brittle fracture due to cleavage, which could not be observed in the present investigation because MVF is lower than 50%.

Finally, the fracture surface analysis verifies the previously obtained conclusions about the energy dissipated by the three materials. As the MVF increases, so does the number and length of secondary microcracks, and hence, the tortuosity and energy dissipated in the fracture surfaces.

4 | CONCLUSIONS

The materials were subjected to crack propagation processes to observe the interaction of the crack with the microstructure. The results obtained with the fracture parameters of the Paris law allow the conclusion that steels with a higher MVF present a more outstanding resistance to crack propagation, reflected in the increase in the magnitude of the Paris law exponent m with the rise in MVF.

The EBSD maps of the crack propagation zone show relevant information about the interaction of crack growth in the microstructure, the strain energy density, and the softening by the propagation of secondary microcracks. Kernel maps show increased tortuosity and energy density at the crack front. The MVF increase produces more significant crack tortuosity and energy required to create the fracture surfaces. Additionally, Taylor maps allow the identification of zones in the microstructure where the propagation of microcracks and accumulated damage generate energy release and reduce the relative yield stress of grains located at the crack front. The fracture surfaces, by the fatigue of the three materials, show the typical signs of striations, which are better defined and more prominent in the material with the highest MVF. Finally, the MVF increase produces a more significant number and extension of secondary microcracks; therefore, the tortuosity and the energy dissipated in the fracture surfaces are greater.

Finally, the results of the fracture energy show a growth of 22.9% between the as-received material and HT3 steel. Increasing the MVF promotes slow crack propagation and requires more energy to propagate in the material. The existence of the two phases in the microstructure promotes a continuous deflection effect of the crack front due to the difference in mechanical properties between ferrite and martensite. The lower fracture toughness of the martensite favors the propagation of the crack front through this phase, for which the increase in its content increases the deflection of the crack front and subtracts its energy as it propagates through the microstructure.

ACKNOWLEDGMENTS

The authors would like to thank the scientific and technical personnel of the Lehrstuhl Werkstofftechnik Institute laboratories and the Ruhr-Universität Bochum for their dedicated support in implementing analytical methods and specimen preparation, especially Professor Prof. Dr.-Ing. W. Theisen, and researchers Dr.-Ing. F. Pohl, Dr.-Ing. J. Krell, and Dr.-Ing. G. Egels. We recognize the support of the Ministerio de Ciencia Tecnología e Innovación of Colombia. We would also like to express gratitude to Mrs. I. Berns support during the project manuscripts development. Special thanks to engineers F. J. Monroy and J. J. Murillo for their insightful advice in numerically treating experimental results and finally, to the Advanced Technical Products Supply Co., Inc., for donating ATP®-641 coating.

DATA AVAILABILITY STATEMENT

The data that support the findings of this study are available from the corresponding author upon reasonable request.

ORCID

D. Avendaño-Rodríguez https://orcid.org/0000-0003-4365-6635

R. Rodriguez-Baracaldo https://orcid.org/0000-0003-3097-9312

L. Mujica-Roncery https://orcid.org/0000-0003-4351-7520

REFERENCES

1. Cantor B, Grant P, Johnston C. *Impact Loading*: Taylor and Francis; 2008.
2. Weng Y, Dong H, Gan Y. *Innovative Steels for Low Carbon Economy*: Springer Berlin Heidelberg; 2011.
3. Fonstein N. *Effect of Structure on Mechanical Properties of Dual-Phase Steels*: Springer; 2015.
4. Tasan CC, Diehl M, Yan D, et al. An overview of dual-phase steels: advances in microstructure-oriented processing and micromechanically guided design. *Ann Rev Mater Res*. 2015;45:391-431.
5. Calcagnotto M, Ponge D, Raabe D. Microstructure control during fabrication of ultrafine grained dual-phase steel: characterization and effect of intercritical annealing parameters. *ISIJ International*. 2012;52:874-883.
6. Zhang J, Di H, Deng Y, Misra RDK. Effect of martensite morphology and volume fraction on strain hardening and fracture behavior of martensite ferrite dual phase steel. *Mater Sci Eng: A*. 2015;627:230-240.
7. Demeri MY. *Dual-Phase Steels*: ASM International; 2013.

8. Nanda T, Singh V, Singh V, Chakraborty A, Sharma S. Third generation of advanced high-strength steels: processing routes and properties. *Proc Inst Mech Eng, Part L: J Mater: Design Appl*. 2019;233:209-238.
9. Sarwar M, Priestner R. Fatigue crack propagation behavior in dual-phase steel. *J Mater Eng Perform*. 1999;8:245-251.
10. Dutta VB, Suresh S, Ritchie RO. Fatigue crack propagation in dual-phase steels: effects of ferritic-martensitic microstructures on crack path morphology. *Metallurgical Trans A*. 1984;15:1193-1207.
11. Sarwar M, Ahmad E, Hussain N, Ahmad B, Manzoor T. Crack path morphology in dual-phase steel. *J Mater Eng Perform*. 2006;15:352-354.
12. Terada D, Ikeda G, Park MH, Shibata A, Tsuji N. Reason for high strength and good ductility in dual phase steels composed of soft ferrite and hard martensite. *IOP Confer Ser: Mater Sci Eng*. 2017;219:12008.
13. Bartz I, Bernshtein AM, Dietrich K. *Qualitative Explanation of Failure Low-Alloy Steels*: Academy of Sciences of the Ukrainian; 1987. No usar como referencia.
14. Bag A, Ray KK, Dwarakadasa ES. Influence of martensite content and morphology on tensile and impact properties of high-martensite dual-phase steels. *Metallurg Mater Trans A*. 1999;30:1193-1202.
15. Avend-Rodrguez D, Granados JD, Espejo-Mora E, Mujica-Roncery L, Rodrguez-Baracaldo R. Fracture mechanisms in dual-phase steel: influence of martensite volume fraction and ferrite grain size. *J Eng Sci Technol Rev*. 2018;11:174-181.
16. Bag A, Ray KK, Dwarakadasa ES. Influence of martensite content and morphology on the toughness and fatigue behavior of high-martensite dual-phase steels. *Metallurgical Mater Trans A*. 2001;32:2207-2217.
17. Kumar S, Curtin WA. Crack interaction with microstructure. *Mater Today*. 2007;10:34-44.
18. Shi J, Zikry MA. Grain-boundary interactions and orientation effects on crack behavior in polycrystalline aggregates. *Int J Solids Struct*. 2009;46:3914-3925.
19. Engel L, Klingele H. *Mechanical Fracture*: Wolfe Science; 1981.
20. Schijve J. *Fatigue as a Phenomenon in the Material*: Springer; 2009.
21. Suresh S. *Fatigue Crack Growth in Ductile Solids*: Cambridge University Press; 1998.
22. Anderson TL. *Fatigue Crack Propagation*. 4ed.: CRC Press/Taylor and Francis Group; 2017.
23. Li S, Kang Y, Kuang S. Effects of microstructure on fatigue crack growth behavior in cold-rolled dual phase steels. *Mater Sci Eng: A*. 2014;612:153-161.
24. Idris R, Prawoto Y. Influence of ferrite fraction within martensite matrix on fatigue crack propagation: an experimental verification with dual phase steel. *Mater Sci Eng: A*. 2012;552:547-554.
25. Sudhakar K, Dwarakadasa E. A study on fatigue crack growth in dual phase martensitic steel in air environment. *Bull Mater Sci*. 2000;23:193-199. https://doi.org/10.1007/BF02719909
26. ASTM-E8/E8M. *Standard Test Methods for Tension Testing of Metallic Materials*: ASTM International; 2016.
27. ASTM-E647. *Standard Test Method for Measurement of Fatigue Crack Growth Rates*: ASTM International; 2015.
28. ASTM-E1820. *Standard Test Method for Measurement of Fracture Toughness*: ASTM International; 2017.
29. Avendao-Rodrguez DF, Rodriguez-Baracaldo R, Weber S, Mujica-Roncery L. Damage evolution and microstructural fracture mechanisms related to volume fraction and martensite distribution on dual-phase steels. *Steel Res Int*. 2022;2022:2200460.
30. Mohanty JR, Verma BB, Ray PK. Prediction of fatigue crack growth and residual life using an exponential model: part II (mode-I overload induced retardation). *Int J Fatigue*. 2009;31:425-432. https://doi.org/10.1016/j.ijfatigue.2008.07.018
31. Mohanty JR, Verma BB, Ray PK. Prediction of fatigue crack growth and residual life using an exponential model: part I (constant amplitude loading). *Int J Fatigue*. 2009;31:418-424. https://doi.org/10.1016/j.ijfatigue.2008.07.015
32. Li S, Zhang Y, Qi L, Kang Y. Effect of single tensile overload on fatigue crack growth behavior in dp780 dual phase steel. *Int J Fatigue*. 2018;106:49-55.
33. Madia M, Vojtek T, Duarte L, Zerbst U, Pokorn P, Jambor M, Huta P. Determination of fatigue crack propagation thresholds for steel in presence of environmental effects. *Int J Fatigue*. 2021;153.
34. Li S, Kang Y, Zhu G, Kuang S. Microstructure and fatigue crack growth behavior in tungsten inert gas welded dp780 dual-phase steel. *Mater Design*. 2015;85:180-189.
35. Sadananda K, Vasudevan AK. *Short Crack Growth Behavior*, Vol. 27: ASTM special technical publication; 1997;301-316. www.astm.org
36. Su M, Xu L, Peng C, Han Y, Zhao L. Fatigue short crack growth, model and EBSD characterization of marine steel welding joint. *Int J Fatigue*. 2022;156.
37. Velasquez CP, Rodriguez DA, Tovar CN, Roncery LM, Baracaldo RR. Fatigue crack growth and fracture toughness in a dual phase steel: effect of increasing martensite volume fraction. *Int J Autom Mech Eng*. 2020;17:8086-8095. https://journal.ump.edu.my/ijame/article/view/3183
38. Tzou JL, Ritchie RO. Fatigue crack propagation in a dual-phase plain-carbon steel. *Scripta Metallurgica*. 1985;19:751-755.
39. Shang JK, Tzou JL, Ritchie RO. Role of crack tip shielding in the initiation and growth of long and small fatigue cracks in composite microstructures. *Metallurgical Trans A*. 1987;18:1613-1627.
40. de Faria GL, Godefroid LB, Nunes IP, de Lacerda JC. Effect of martensite volume fraction on the mechanical behavior of an UNS s41003 dual-phase stainless steel. *Mater Sci Eng A*. 2020;797.
41. Sun L, Li S, Zang Q, Wang Z. Dependence of fatigue crack closure behavior on volume fraction of martensite in dual-phase steels. *Scripta Metallurgica et Materialia*. 1995;32:517-521.
42. Wasn J, Karlsson B. Influence of prestrain and ageing on near-threshold fatigue crack growth in fine-grained dual-phase steels. *Int J Fatigue*. 1989;11:395-405.
43. Zhang Z, Yue Z, Qi J, Gao J, Qiu Y. Low cycle fatigue performance of dp900 steel under cyclic shear paths. *Fatigue Fract Eng Mater Struct*. 2022;45:22-39.
44. Tayanç M, Ayta A, Bayram A. The effect of carbon content on fatigue strength of dual-phase steels. *Mater Design*. 2007;28:1827-1835.

45. Mosselman W. *The Influence of the Martensite Content on the Fatigue Crack Growth Rate in Trip and Dual Phase Steels, Master Thesis*: Delft University of Technology; 2007.
46. Tkach AN, Fonshteln NM, Simin'kovich VN, Bortsov AN, Lenets YN. Fatigue crack growth in a dual-phase ferritic-martensitic steel. *Khimicheskaya Mekhanika Materialov*. 1985; 20:448-453.
47. Zhu XK, Joyce JA. Review of fracture toughness (g, k, j, CTOD, CTOA) testing and standardization. *Eng Fract Mech*. 2012;85: 1-46.
48. Mochizuki M, Kohara M, Shimanuki H, Hagiwara Y, Toyoda M. Crack initiation and propagation in ferrite/martensite dual-phase steel with microscopic heterogeneity by fracture toughness tests. *Zairyo*. 2003;52:932-938.
49. Qi X, Du L, Dong Y, Misra RDK, Du Y, Wu H, Gao X. Fracture toughness behavior of low-c medium-mn high-strength steel with submicron-scale laminated microstructure of tempered martensite and reversed austenite. *J Mater Sci*. 2019;54:12095-12105.
50. Ambrisko L, Pesek L. The crack growth resistance of thin steel sheets under eccentric tension. *Sādhanā*. 2018;43:1-8.
51. Tian C, Kirchlechner C. The fracture toughness of martensite islands in dual-phase dp800 steel. *J Mater Res*. 2021;36:2495-2504.
52. Huang J, Li S, Zhong H, Li D, Zhang Z. Effects of notch position on the fatigue crack growth behavior of dissimilar laser welded dp980/qp980 joint. *Fatigue Fract Eng Mater Struct*. 2022;45:1111-1125.

How to cite this article: Avendaño-Rodríguez D, Rodriguez-Baracaldo R, Weber S, Mujica-Roncery L. Martensite content effect on fatigue crack growth and fracture energy in dual-phase steels. *Fatigue Fract Eng Mater Struct*. 2023; 1-19. doi:10.1111/ffe.14209